Magnetic properties of point defects in iron within the tight-binding-bond Stoner model

Guoqiang Liu,[1,2] D. Nguyen-Manh,[2,3] Bang-Gui Liu,[1] and D. G. Pettifor[2]
[1]*Institute of Physics, Center of Condensed Matter Physics, Chinese Academy of Sciences, P.O. Box 603, Beijing 100080, China*
[2]*Department of Materials, University of Oxford, Parks Road, Oxford OX1 3PH, United Kingdom*
[3]*UKAEA Culham Division, Culham Science Centre, Abingdon OX14 3DB, United Kingdom*
(Received 28 December 2004; revised manuscript received 14 March 2005; published 31 May 2005)

The tight-binding Stoner model of band magnetism is generalized to account for local charge neutrality by working within the tight-binding-bond (TBB) representation of the binding energy. We show that the analytic forces within this TBB Stoner model take a very simple form because neither the renormalization in the on-site energies due to local charge neutrality nor the change in local magnetic moments due to atomic displacement enters explicitly. This *d* band TBB Stoner model is found to reproduce qualitatively the variations in local moments on and around point defects that are predicted by first principles density functional theory. In agreement with experiments, the formation energies show that the most stable self-interstitial defect is the $\langle 110 \rangle$ dumbbell.

DOI: 10.1103/PhysRevB.71.174115 PACS number(s): 61.72.Bb, 71.15.Nc, 71.20.Be

I. INTRODUCTION

Point defects play a critical role in the evolution of the mechanical properties of metals under neutron irradiation, their aggregation into voids or clusters leading to swelling and creep, and possible structural failure. It is, therefore, not surprising with the renewed worldwide interest in fusion power that attention is focusing on those structural materials with promising irradiation resistance, namely alloys based on the bcc transition metals vanadium[1] or iron.[2] Recently, computationally intensive first-principles density-functional theory (DFT) calculations have been performed on the energetics of point defects in vanadium, predicting that the $\langle 111 \rangle$ dumbbell is the most stable self-interstitial with a formation energy of 3.1 eV.[3] This *ab initio* DFT database has then been used to fit an interatomic Finnis-Sinclair potential for vanadium[4] which has allowed the molecular dynamics simulation of the threshold displacement energy,[5] a first step towards modeling the behavior of the displacement cascades.[6]

Modeling damage evolution in bcc iron under neutron irradiation, however, is complicated by the presence of magnetism. As is well known, the stability of the bcc α-phase is driven by the large magnetic energy of 0.5 eV/atom,[7] which overcomes the preference for the hcp structure displayed by the nonmagnetic isovalent 4*d* and 5*d* elements ruthenium and osmium (and indeed also the high pressure ϵ-phase of iron). Spin-polarized DFT calculations have demonstrated that the local moment on an iron atom is very sensitive to its environment. For example, the magnetic moment on the $\langle 110 \rangle$ dumbbell self-interstitial is predicted to be reduced by 90% in magnitude and have opposite spin direction to the bulk magnetization.[8] This nonparallel alignment and low spin state of the moment is reminiscent of the experimental and theoretical behavior of the fcc γ-phases of iron and its invar alloys.[9–12] Unfortunately, this sensitivity of the local magnetic moment to its atomic environment implies that it will be difficult to find a single, simple interatomic potential that will be able to simulate damage evolution reliably in bcc iron or the more complex ferritic steels.[2] Proper recognition must be given to a better understanding and description of the magnetic contribution to the binding energy.

The tight-binding (TB) approximation provides a natural framework for bridging between the first-principles DFT calculations and the semiempirical interatomic potentials for nonmagnetic materials. By coarse graining the TB electronic structure in terms of atom-centered moments and bond-centered interference paths[13] interatomic bond-order potentials (BOPs) may be derived that correctly predict (rather than fit) the observed structural trends across the periodic table of elements.[14] For the *sp* valent elements, analytic BOPs have been obtained that handle the bond breaking and remaking that occurs during film growth.[15] For the *d* valent transition metals and intermetallics, numerical BOPs have been used to model dislocation behavior.[16–18]

The Stoner model of band magnetism[19] allows the TB approximation to be generalized to magnetic materials. This model of itinerant magnetism has been justified from the density functional theory.[20] Twenty-one years ago Hasegawa and Pettifor[21] showed that a finite-temperature theory of band magnetism, including only *d* states, could account qualitatively for the experimental P-T phase diagram of iron with its occurrence of the α(bcc), γ(fcc), δ(bcc), and ϵ(hcp) phases. More recently, a *d*-state TB Stoner model has been applied successfully to model planar defects in bcc iron by Yesilleten *et al.*[22] They found that the intergranular cohesion along symmetric tilt boundaries depended strongly on the magnetic structure at the interface, the local moments being enhanced by up to 18% compared to the bulk.

In this paper we generalize the TB Stoner model of band magnetism to include charge self-consistency, which is important for a realistic treatment of point defects. In particular, as we are dealing with metallic systems with perfect screening, we will assume that each atom remains locally charge neutral (LCN). This is achieved by adjusting the on-site energies up or down until all the atoms have zero net charge.[23] In order for this self-consistent TB model to satisfy the frozen potential or force theorem,[24,25] we must work within the TB bond representation for the binding energy[26–29] rather than the conventional TB band representation. This guaran-

tees that the renormalization or shift in the on-site energies does not enter the TB expression for the force.

The plan of the paper is as follows. We derive the TB bond Stoner model in the next section. We then present the results for iron in Sec. III, retaining only the valence *d* states. In Sec. III A we calculate the bulk properties of pure iron. The energies, equilibrium atom volume, magnetic moment, and elastic constants are presented for three different structures bcc, fcc, and hcp. In Sec. III B we use the TB *d* bond Stoner model to predict the formation energies and local magnetic structures of vacancies and self-interstitials in bcc iron. In Sec. IV we conclude.

II. TIGHT-BINDING-BOND STONER MODEL

The TB bond model was introduced in order to handle local charge neutrality within metallic binary alloys[27] and compounds.[26] For nonmagnetic systems, the binding energy within density functional theory (DFT) can be written as

$$E_{DFT} = E_{band} - E_{dc} + E_{ii} - E_{atom}. \tag{1}$$

The first term is obtained by summing over all the occupied eigenstates in the band, the second term is the usual double counting correction for the electron-electron interactions, the third term is the ion-ion repulsion (assuming the core electrons have been pseudized away), and the last term is the energy of the atoms when they are removed to infinity. Within the conventional TB band model the second and third contributions in Eq. (1) are grouped together as a single pairwise repulsive term. If LCN is now introduced, then the resultant shifts in the on-site energies will affect only the band contribution and not this empirical repulsive pairwise term. This immediately implies that the TB band model fails to satisfy the frozen potential or force theorem,[24,25] which states that the first order change in the band energy contribution is exactly cancelled by a similar shift in the double counting term in Eq. (1)

The TB bond (TBB) model avoids this problem by separating out the on-site and inter-site contributions within the band energy. The former term is grouped with the double counting and ion-ion contributions, which together now represent the electrostatic interaction between overlapping neutral atoms.[28,29] Within the orthogonal TBB model, this electrostatic interaction is further grouped with the overlap repulsion and represented empirically by a single repulsive pairwise contribution.[30] The TBB binding energy for a nonmagnetic (NM) system can then be written in the physically intuitive form as

$$E_{TBB}^{NM} = E_{bond}^{NM} + E_{prom} + E_{rep}, \tag{2}$$

where all atoms are constrained to be LCN.

The nonmagnetic bond energy is given by

$$E_{bond}^{NM} = 2\sum_{i\alpha} \int^{\epsilon_F} (\epsilon - \epsilon_{i\alpha}^0) n_{i\alpha}(\epsilon) d\epsilon, \tag{3}$$

where the prefactor 2 accounts for the spin-degeneracy of the nm state and ϵ_F is the Fermi energy. $\epsilon_{i\alpha}^0$ and $n_{i\alpha}$ are the on-site energy and local density of states, respectively, associated with orbital α on site i. This can be decomposed in terms of the individual bond energies between orbitals α and β on neighboring sites u and j, namely

$$E_{bond}^{NM} = 2 \sum_{\substack{i\alpha,j\beta \\ (i\neq j)}} \rho_{i\alpha,j\beta} H_{j\beta,i\alpha}, \tag{4}$$

where the prefactor 2 accounts for the spin degeneracy of the nonmagnetic state. $\rho_{i\alpha,j\beta}$ and $H_{j\beta,i\alpha}$ are elements of the density matrix, and two-center orthogonal TB Hamiltonian matrix, respectively. Thus an individual bond energy is given by the product of an intersite Hamiltonian matrix element and corresponding density matrix or bond order,[13–18] as Coulson showed in 1939.[31]

The second term in Eq. (2) is the promotion energy. For an *sd* band model this would take the form

$$E_{prom} = \sum_i (\epsilon_d^0 - \epsilon_s^0) \Delta N_{id} \tag{5}$$

if the nonmagnetic *s*-*d* atomic energy level splitting $(\epsilon_d^0 - \epsilon_s^0)$ is assumed to take a fixed value for a given element. ΔN_{id} gives the change in the number of *d* electrons associated with site *i* compared to the free atom state. Due to LCN we have $\Delta N_{is} = -\Delta N_{id}$. For a pure *d* band model the promotion energy is zero. Finally, the last term in Eq. (2) is usually represented by a simple repulsive pairwise contribution, although for more quantitative predictions of defect behavior it may take a more complicated many-body form (see, for example, Refs. 16–18.)

The Stoner model introduces magnetism by including the presence of local exchange fields within the band energy of Eq. (1). In particular, for collinear magnetic states, up and down spin electrons will see different on-site energies according to whether their spin is parallel or antiparallel to the local magnetic moment. Defining I as the Stoner exchange integral, the local on-site energies for the *d*-band model take the form

$$\epsilon_{id}^{\sigma} = \epsilon_{id}^0 \pm \frac{1}{2} I m_i, \tag{6}$$

where m_i is the difference in the number of *d* electrons on site *i* with spin parallel and antiparallel to the local moment, respectively. The minus (plus) sign is taken if the spin σ is parallel (antiparallel) to the direction of the local magnetic moment. The local exchange splitting on atom *i*

$$\Delta_i = I m_i \tag{7}$$

is then determined self-consistently so that the magnetic moment m_i predicted as output implies from Eq. (7) the same exchange field Δ_i as used as input. The above collinear model can be easily generalized to include noncollinear magnetic states[32–34] such as those observed in the fcc γ-phase of iron.[10,12]

The binding energy within the TBB model can now be extended to treat magnetism by including the exchange fields within the band energy and subtracting off in Eq. (1) the double counting Stoner exchange energy E_X, where

$$E_X = -\frac{1}{4}\sum_i I m_i^2. \tag{8}$$

This leads to the expected TBB form:

$$E_{TBB} = E_{bond} + (E_X - E_X^{atom}) + E_{prom} + E_{rep}, \tag{9}$$

where

$$E_{bond} = \sum_{\sigma=\uparrow,\downarrow} \sum_{\substack{i\alpha,j\beta \\ (i\neq j)}} \rho^{\sigma}_{i\alpha,j\beta} H_{j\beta,i\alpha} \tag{10}$$

and

$$E_X - E_X^{atom} = -\frac{1}{4}\sum_i I(m_i^2 - m_{atom}^2) \tag{11}$$

with m_{atom} being the magnetic moment of the free atom. For the ferromagnetic state, Eq. (9) is equivalent to the well-known Stoner result,[19] the first term resulting in the increase in kinetic energy on flipping the spins from the minority to majority band, the second term representing the corresponding gain in exchange energy.

The forces may be easily evaluated. The TBB binding energy, Eq. (9), may be rewritten as

$$E_{TBB} = \sum_{\sigma=\uparrow,\downarrow} \sum_{i\alpha,j\beta} \rho^{\sigma}_{i\alpha,j\beta} H^{\sigma}_{j\beta,i\alpha} - \sum_{i\alpha} \rho^{\sigma}_{i\alpha,i\alpha} \epsilon^{\sigma}_{i\alpha} + (E_X - E_X^{atom}) + E_{prom} + E_{rep} \tag{12}$$

since for $i=j$ we have $H^{\sigma}_{i\alpha,j\beta} = \epsilon^{\sigma}_{i\alpha}\delta_{\alpha\beta}$. Therefore, differentiating with respect to an atomic coordinate $\mathbf{r}_k$, the force on atom k is given by

$$\mathbf{F}_k = -\sum_{\sigma=\uparrow,\downarrow} \sum_{i\alpha,j\beta} \rho^{\sigma}_{i\alpha,j\beta} \frac{\partial H^{\sigma}_{j\beta,i\alpha}}{\partial \mathbf{r}_k} + \frac{\partial E_X}{\partial \mathbf{r}_k} - \frac{\partial E_{rep}}{\partial \mathbf{r}_k}. \tag{13}$$

The first term in Eq. (13) is the usual Hellmann-Feynman force resulting from the first contribution in Eq. (12). The second term in Eq. (13) is the derivative of the double counted exchange energy resulting from combining the second and third terms in Eq. (12). The promotion energy does not contribute to the force within the LCN model provided $\epsilon_d^0 - \epsilon_s^0$ remains constant.[23,28] Finally, it follows from Eqs. (6) and (8) that the on-site contribution in the first term of Eq. (13) cancels the derivative of the double counted exchange term. Hence we recover the simple expression for the force within the TBB model

$$\mathbf{F}_k = -\sum_{\sigma=\uparrow,\downarrow} \sum_{i\alpha\neq j\beta} \rho^{\sigma}_{i\alpha,j\beta} \frac{\partial H^{\sigma}_{j\beta,i\alpha}}{\partial \mathbf{r}_k} - \frac{\partial E_{rep}}{\partial \mathbf{r}_k}. \tag{14}$$

We see at once that the first-order shifts in the on-site energies do not enter Eq. (14) so that the TBB representation satisfies the frozen potential or force theorem.[24,25] Moreover, since the local exchange fields and moments have all been determined self-consistently through Eq. (7), the binding energy is stationary with respect to either Δ_i or m_i. Hence, although the local moments and exchange fields are sensitive to small displacements of an atom, these changes do not enter the TBB force in Eq. (14). Thus the forces are immediately available for atomistic relaxations or MD simulations once the density matrix (or bond-order matrix) has been obtained. We have implemented this scheme by using the k-space routine in the OXON code,[35] which we have generalized to include magnetism within the TBB Stoner model as described above. We have not used the order N routine within the OXON code because the k-space method provides not only exact Hellmann-Feynman forces for relaxation of the defects, but also very accurate DOS about the Fermi level for treating the presence of magnetism.

III. RESULTS

A. Bulk properties

We begin by fitting the TBB model to the equilibrium bulk properties of bcc iron. We retain only the valence d orbitals within the basis as there is no clear improvement if a more complex model, such as sd, is introduced.[36] We assume that the repulsive energy is described by the sum of a short-range Yukawa potential plus a longer range exponential, namely

$$E_{rep} = \frac{1}{2}\sum_{i,j}\left(\frac{B}{r_{ij}^m} e^{-qr_{ij}} + Ae^{-pr_{ij}}\right), \tag{15}$$

where A, B, p, q, and m are fitting parameters. The $dd\sigma$, $dd\pi$, and $dd\delta$ bond integrals are approximated by a power law, namely

$$t(r) = t(r_0)(r/r_0)^{-n}, \tag{16}$$

where r_0 is the equilibrium nearest-neighbor bond length of the bcc ferromagnetic ground state of iron.

Initial values of the bond integrals were obtained using the third-generation LMTO method which accurately reproduces the DFT band structure of transition metals within a minimal basis set.[37] The resultant bond integrals lead to d band densities of states for the bcc, fcc, and hcp crystal structures that predict within a Jones-type analysis the observed structural trends across the transition metal series.[38] The number of d electrons N_d was taken from these LMTO calculations for nonmagnetic bcc iron. We chose the initial value of the Stoner exchange integral $I=0.632$ eV, which Zhong *et al.*[39] found reproduced the experimental magnetic moment of bcc iron within their sd TB Stoner model. Initial values of the repulsive parameters were then found by finding the best fit to the experimental equilibrium volume and elastic moduli of bcc iron and the DFT energy difference between nonmagnetic fcc iron and ferromagnetic bcc iron.[7] All the parameters were then reoptimized together to fit the above experimental and DFT data within the d TBB model.

Table I gives the resultant parameters. The exponents n of the dd hopping integrals are close to the value of 5 which was predicted by Heine[40] from a simple approximation within resonant scattering theory. The corresponding nonmagnetic density of states (DOS) for bcc, fcc, and hcp are shown in Fig. 1. As expected, these d band DOS mirror very closely those for canonical d bands.[41]

The resultant TB binding energy curves relative to the ferromagnetic (FM) bcc ground state energy are shown as a

TABLE I. Tight-binding, exchange, and repulsive energy parameters fitted within the *d* approximation to the TBB Stoner model, respectively. N_d gives the number of *d* electrons. The data in the bond integrals columns give the bcc first nearest-neighbor equilibrium value t_0 (eV) and the exponent *n*. The repulsive energy parameters are listed according to Eq. (15).

	N_d	I (eV)	$dd\sigma$	$dd\pi$	$dd\delta$
Values	6.8	0.77	−0.6877	0.4196	−0.0392
Exponent *n*			4.5	4.0	4.0
	A(eV)	p(Å^{-1})	B(eV)	m	q(Å^{-1})
Values	-8.62×10^4	2.92	1.2×10^5	1	2.68

function of atomic volume in Fig. 2 for the nonmagnetic (NM), antiferromagnetic (AFM), and FM metastable phases of iron with respect to fcc and bcc in the left-hand panel and hcp and bcc in the right-hand panel. These TB curves reflect the trends displayed by DFT in Figs. 2 and 6 of Ref. 7, respectively. However, the specific equilibrium energy values listed in Table II demonstrate that this comparison between TB and DFT is at best qualitative. For example, the TB magnetic energy of the bcc FM phase is found to be 38% too small compared to DFT.

Figure 3 shows that the magnetic moments for the FM and AFM phases behave in the way observed in Ref. 7 as the volume decreases. In particular, the moment collapses precipitously as a step-function in the FM hcp phase, whereas it collapses more gently as the square root in the AFM fcc and hcp phases. The much larger value of the AFM hcp moment predicted by TB compared to DFT in Table II is a direct consequence of the TB equilibrium volume being 6% larger and hence moving the very small DFT moment up the square root singularity in Fig. 3.

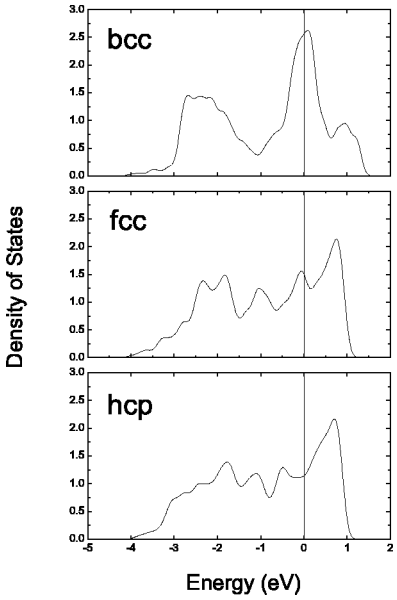

FIG. 1. Nonmagnetic *d* band density of states for bcc, fcc, and hcp structures. The zero of energy is taken at the Fermi energy which corresponds to 6.8 *d* electrons.

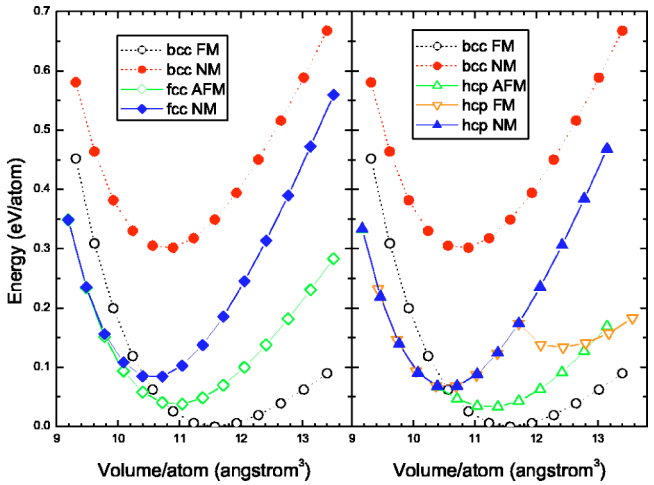

FIG. 2. (Color online) Binding energy curves relative to the ferromagnetic (FM) bcc ground state energy for nonmagnetic (NM), antiferromagnetic (AFM), and FM metastable phases of iron with respect to fcc (hcp) and bcc in the left- (right-) hand plane.

Table III shows that this TB model gives reasonably quantitative values for the shear moduli of the FM bcc ground state phase of iron, which is not unexpected given that the experimental values were used in the fit. Importantly, however, the TB model predicts that the NM bcc phase has a negative value of the tetragonal shear modulus. This agrees with other TB and DFT results that find the NM bcc structure of group VIII transition metals to be mechanically unstable.[45,46]

B. Points defects

The formation energy of a point defect is calculated from

$$\Delta E = E_{def}(N_{def}) - \frac{N_{def}}{N}E(N), \tag{17}$$

where N_{def} and N are the number of atoms per unit cell in the defect structure and perfect lattice, respectively. $E_{def}(N_{def})$

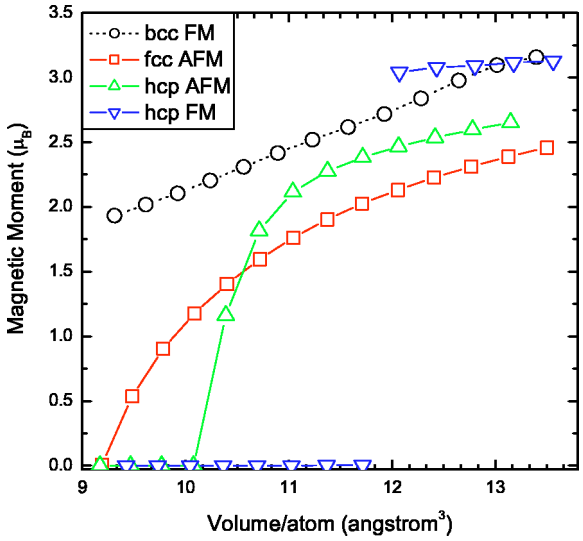

FIG. 3. (Color online) Magnetic moments of iron as functions of atomic volume.

TABLE II. Calculated equilibrium atomic volume (Å^3), energy relative to the bcc ground state (eV/atom), bulk modulus (GPa), and magnetic moment (μ_B/atom) for nonmagnetic (NM), ferromagnetic (FM), and antiferromagnetic (AFM) phases of iron with respect to the bcc, fcc, and hcp structures. Experimental and density functional theory (DFT) predictions are from Refs. 42 and 7, respectively. The DFT results for FM hcp iron are given for the high spin state (Ref. 7).

	Volume (Å^3)	ΔE (eV/atom)	B (Gpa)	μ (μ_B/atom)
		bcc-Fe		
FM bcc				
TBB	11.57	0	168	2.62
DFT	11.44	0	174	2.17
Experiment	11.70	0	172	2.22
NM bcc				
TBB	10.73	0.30	314	0
DFT	10.59	0.48	276	0
		fcc-Fe		
AFM fcc				
TBB	10.84	0.04	219	1.59
DFT	10.69	0.10	193	1.30
NM fcc				
TBB	10.70	0.09	328	0
DFT	10.34	0.15	293	0
		hcp-Fe		
AFM hcp				
TBB	11.04	0.04	144	2.04
DFT	10.40	0.10	202	0.37
NM hcp				
TBB	10.39	0.06	338	0
DFT	10.32	0.08	291	0
FM hcp				
TBB	12.41	0.13	131	3.07
DFT	12.03	0.22	174	2.55

and $E(N)$ are the corresponding total binding energies per unit cell. The defect formation volume is calculated using the method of Simonelli *et al.*,[47] in which the Kanzaki forces are computed to obtain the dipolar tensor P. The defect relaxation volume $\Delta\Omega$ is given by Tr $(P)/3B$, where B is the bulk modulus. The vacancy formation volume is then

$$\Omega_v^f = \Omega_0 + \Delta\Omega, \tag{18}$$

where Ω_0 is the atomic volume of the perfect lattice.

TABLE III. Shear moduli of bcc iron. Experimental and density functional theory (DFT) results from Refs. 43 and 44, respectively.

	C' (Gpa)	C_{44} (Gpa)
NM		
TBB	−158	178
DFT	−110	141
FM		
TBB	36	118
DFT	69	99
Experiment	43	116

The point defect calculations presented below used 216 k points for the 54 atom unit cells, 125 k points for the 128 atom unit cells, and 64 k points for the 250 atom unit cells. We checked the convergence of the energies and forces with respect to the number of k points. We found that the number of k points quoted above allow five significant figures for the binding energy and four significant figures for the force on individual atoms.

1. Vacancy

The formation energy and formation volume of a single vacancy are shown in Table IV. We see that our TBB Stoner model predicts a vacancy formation energy that is 14% smaller than the DFT value[8] but which lies within the two experimental values.[48,49] The vacancy formation volume is in good agreement with both DFT and experiment.[42] A comparison of the TBB and DFT atomic shell relaxations about the vacancy is illustrated in Fig. 4. We see that the TBB predictions underestimate the amount of relaxation of the first neighbor shell, but reflect the oscillatory behavior over more distant neighbors.

The behavior of the local magnetic moments about an unrelaxed vacancy is shown in Fig. 5. As expected, we find that LCN damps down the amplitude and range of oscillations about the vacancy compared to the case without LCN.

TABLE IV. Vacancy and self-interstitial formation energies (eV) and vacancy formation volume (per atomic volume) of bcc iron. E_{vac}^{un} is unrelaxed vacancy formation energy. Two experimental values of vacancy formation energy are from Refs. 48 and 49, respectively, whereas experimental formation volume is from Ref. 50. Density functional theory (DFT) values are from Refs. 8 and 51.

	E_{vac}^f	E_{vac}^{un}	Ω_v^f/Ω_0	$E^f\langle 100\rangle$	$E^f\langle 110\rangle$	$E^f\langle 111\rangle$
TBB (54 atoms)	1.68	1.75	0.93	5.37	4.36	4.72
TBB (128 atoms)	1.66	1.74	0.92	5.13	4.28	4.55
TBB (250 atoms)	1.65	1.74	0.92	5.11	4.25	4.52
DFT Ref. 8 (54 atoms)	1.95	2.24	0.90	4.37	3.41	4.11
DFT Ref. 49 (128 atoms)	2.07			4.64	3.64	4.34
Experiment	1.53,2		0.95			

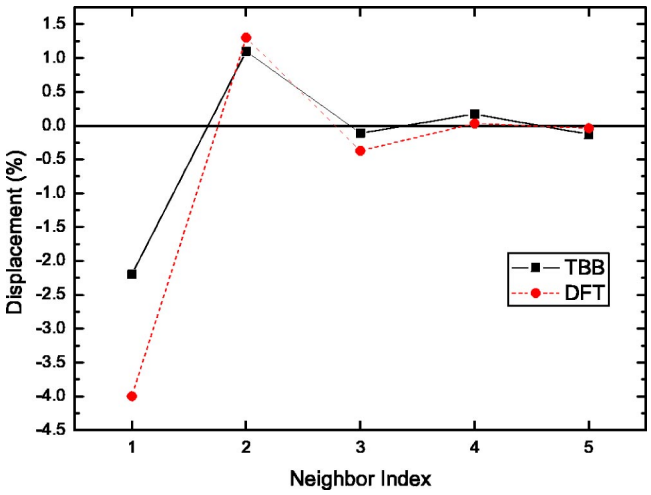

FIG. 4. (Color online) Nearest-neighbor shell relaxations about a vacancy at the center of a 53 atom unit cell within the TBB model with LCN (full curve) and DFT (dashed curve). The latter values are from Ref. 8.

2. Self-interstitials

The formation energies of the ⟨100⟩, ⟨110⟩, and ⟨111⟩ dumbbell self-interstitials are presented in Table IV. The structures were relaxed at the equilibrium volume of the bcc FM state. We see that the convergence with respect to cell size is fast, as previous studies have also observed.[8] The distances between the two dumbbell atoms in their relaxed configurations are found to be 1.97, 1.92, and 1.85 Å for the ⟨100⟩, ⟨110⟩, and ⟨111⟩ dumbbells, respectively. The other atoms around the point defect are only slightly perturbed, which are displaced by less than 0.25 Å, apart from the ⟨111⟩ neighbors of the ⟨111⟩ dumbbell which more outwards by 0.61 Å. We see that the *d* approximation to the TBB Stoner model overestimates the formation energies by about 20% compared to the DFT values.[8] Nevertheless, the relative stability of the three dumbbells is maintained with the ⟨110⟩ predicted as the most stable in agreement with experiment.[50,51]

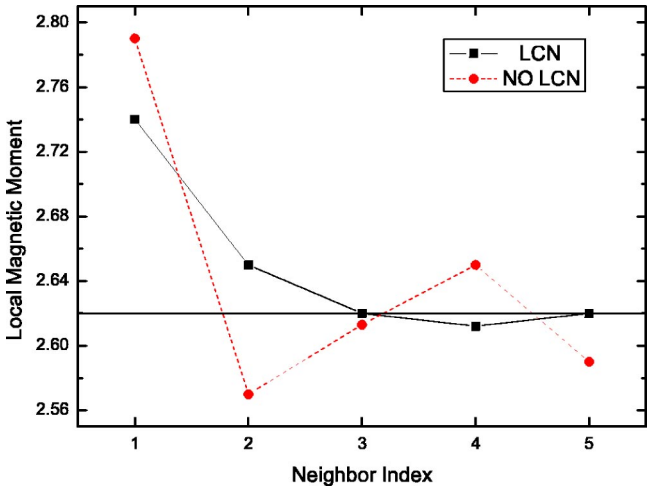

FIG. 5. (Color online) Local magnetic moments on neighboring atoms about unrelaxed vacancy at the center of a 53 atom unit cell within the TBB model with LCN (full curve) and without LCN (dashed curve).

TABLE V. TBB and DFT (Ref. 8) values of the local magnetic moment of the dumbbell atoms and their neighbors for a 129 atom unit cell.

		Moment (μ_B/atom)		
	Neighbor	⟨100⟩	⟨110⟩	⟨111⟩
TBB	dumbbell	0.17	−0.20	0.18
DFT		0.18	−0.18	0.28
TBB	111	2.26	0.84	0.73
DFT		2.25	1.87	1.16
TBB	$11\bar{1}$	2.26	0.84	2.65
DFT		2.25	1.87	2.41
TBB	$1\bar{1}1$	2.26	2.73	2.65
DFT		2.25	2.52	2.41
TBB	$\bar{1}11$	2.26	2.73	2.65
DFT		2.25	2.52	2.41

The behavior of the local magnetic moment on the dumbbell atoms and their neighbors is given in Table V for a 129 atom until cell. We see that the *d* approximation to the TBB Stoner model qualitatively reproduces the DFT[8] variations in moments about the three defects. In particular, it finds the antiparallel alignment of the ⟨110⟩ dumbbell moment compared to the bulk direction that was first predicted by DFT.[8]

IV. CONCLUSION

We have generalized the tight-binding Stoner model of band magnetism to account for local charge neutrality, which is essential for a proper treatment of defects in metals. This requires working within the TB bond representation of the binding energy rather than the conventional TB band representation, in order to satisfy the Pettifor-Andersen force theorem. We have shown that the analytic forces within this TBB Stoner model still take a very simple form because neither the renormalization in the on-site energies due to local charge neutrality nor the change in local magnetic moments due to atomic displacement enters explicitly.

We have applied this TBB Stoner model to a study of the point defects in ferromagnetic bcc iron, retaining only the valence *d* orbitals within the bonding contribution. We find that the results qualitatively reproduce the variations in the local magnetic moments on and around defects which are predicted by density functional theory. However, the magnitude of the vacancy formation energy is 15% too small and that of the dumbbell self-interstitials 20% too large. Future work will introduce a more accurate description of the environmental dependence of both the bond integrals[52] and repulsive energy[16] in order to ensure their better transferability. This more robust TBB Stoner model should allow the magnetic energies of iron atoms in different local environments to be rapidly calculated and fitted by a simple analytic ex-

pression. This magnetic potential in conjunction with a non-magnetic bond-order potential could then be applied to simulating atomistically radiation damage in bcc iron and its alloys.

ACKNOWLEDGMENTS

We would like to acknowledge useful discussions with Sergei Dudarev and Andrew Horsfield. This work is supported by UK Royal Society and the Chinese Academy of Sciences through a collaborative project. Guoqiang Liu and Bang-Gui Liu would like to acknowledge support from Natural Science Foundation of China (90406010, 60021403). D. Nguyen-Manh would like to acknowledge the fundings from the United Kingdom Engineering and Physical Science Research Council (EPSRC) and EURATOM. We thank the Oxford Supercomputing Centre for use of their facilities.

[1] H. M. Chung, B. A. Loomis, and D. L. Smith, J. Nucl. Mater. **239**, 139 (1996).
[2] A. Hishinuma, A. Kohyama, R. L. Klueh, D. S. Gelles, W. Dietz, and K. Ehrlich, J. Nucl. Mater. **258-263**, 193 (1998).
[3] S. Han, L. A. Zepeda-Ruiz, G. J. Ackland, R. Car, and D. J. Srolovitz, Phys. Rev. B **66**, 220101(R) (2002).
[4] S. Han, L. A. Zepeda-Ruiz, G. J. Ackland, R. Car, and D. J. Srolovitz, J. Appl. Phys. **93**, 3328 (2003).
[5] L. A. Zepeda-Ruiz, S. Han, D. J. Srolovitz, R. Car, and B. D. Wirth, Phys. Rev. B **67**, 134114 (2003).
[6] D. J. Bacon, F. Gao, and Yu. N. Osetsky, J. Nucl. Mater. **276**, 1 (2000).
[7] H. C. Herper, E. Hoffmann, and P. Entel, Phys. Rev. B **60**, 3839 (1999).
[8] C. Domain and C. S. Becquart, Phys. Rev. B **65**, 024103 (2001).
[9] L. Kaufman, E. V. Clougherty, and R. J. Weiss, Acta Metall. **11**, 323 (1963).
[10] Y. Tsunoda, Y. Nishioka, and R. M. Nicklow, J. Magn. Magn. Mater. **128**, 133 (1993).
[11] D. M. Roy and D. G. Pettifor, J. Phys. F: Met. Phys. **7**, L183 (1977).
[12] K. Knöpfle, L. M. Sandratskii, and J. Kübler, Phys. Rev. B **62**, 5564 (2000).
[13] D. G. Pettifor and M. Aoki, Philos. Trans. R. Soc. London, Ser. A **334**, 429 (1991).
[14] R. Drautz, D. Nguyen-Manh, D. A. Murdick, X. W. Zhou, H. N. G. Wadley, and D. G. Pettifor, *3rd International Conference on Computational Modeling and Simulation of Materials, Part B*, edited by F. Vincenzini, and A. Lami, Techna Group Srl., 231–442 2004.
[15] D. G. Pettifor and I. I. Oleinik, Phys. Rev. Lett. **84**, 4124 (2000).
[16] M. Mrovec, D. Nguyen-Manh, D. G. Pettifor, and V. Vitek, Phys. Rev. B **69**, 094115 (2004).
[17] S. Znam, D. Nguyen-Manh, D. G. Pettifor, and V. Vitek, Philos. Mag. **83**, 415 (2003).
[18] M. J. Cawkwell, D. Nguyen-Manh, V. Vitek, and D. G. Pettifor, in *Multiscale Phenomena in Materials-Experiments and Modeling Related to Mechanical Behavior*, edited by H. M. Zbib *et al.*, Mat. Res. Soc. Symposium Proceedings Series (Materials Research Society, Warrendable, 2003), 779, W.5.5.
[19] E. C. Stoner, Philos. Trans. R. Soc. London, Ser. A **169**, 339 (1939).
[20] O. Gunnarsson, J. Phys. F: Met. Phys. **6**, 587 (1976).
[21] H. Hasegawa and D. G. Pettifor, Phys. Rev. Lett. **50**, 130 (1983).
[22] D. Yesilleten, M. Nastar, T. A. Arias, A. T. Paxton, and S. Yip, Phys. Rev. Lett. **81**, 2998 (1998).
[23] A. P. Horsfield, A. M. Bratkovsky, M. Fearn, D. G. Pettifor, and M. Aoki, Phys. Rev. B **53**, 12694 (1996).
[24] D. G. Pettifor, Commun. Phys. (London) **1**, 141 (1976).
[25] A. R. Mackintosh and O. K. Andersen, in *Electrons at the Fermi Surface*, edited by M. Springford (Cambridge University Press, Cambridge, 1980), section 5.3.
[26] D. G. Pettifor and R. Podloucky, J. Phys. C **19**, 315 (1986).
[27] D. G. Pettifor, Solid State Phys. **40**, 43 (1987).
[28] A. P. Sutton, M. W. Finnis, D. G. Pettifor, and Y. Ohta, J. Phys. C **21**, 35 (1988).
[29] D. G. Pettifor, Springer Proc. Phys. **48**, 64 (1990).
[30] A. J. Skinner and D. G. Pettifor, J. Phys.: Condens. Matter **3**, 2029 (1991).
[31] C. A. Coulson, Philos. Trans. R. Soc. London, Ser. A **169**, 413 (1939).
[32] J. Hubbard, Phys. Rev. B **19**, 2626 (1979).
[33] D. G. Pettifor, J. Magn. Magn. Mater. **15-18**, 847 (1980).
[34] M. Van Schilfgaarde and V. P. Antropov, J. Appl. Phys. **85**, 4827 (1999).
[35] A. P. Horsfield, D. R. Bowler, A. M. Bratkovsky, M. Fearn, P. Goodwin, S. Goedecker, C. Gorringe, D. Muller, R. Harris, and D. Nguyen-Manh, *OXON code* (University of Oxford, Oxford, England, 2001). See also URL http://www-mml.materials.ox.ac.uk/facilities/oxon.shtml.
[36] A. T. Paxton, J. Phys. D **29**, 1689 (1996).
[37] D. Nguyen-Manh, T. Saha-Dasgupta, and O. K. Andersen, Bull. Mater. Sci. **26**, 27 (2003).
[38] D. Nguyen-Manh, S. L. Dudarev, G. Q. Liu, and D. G. Pettifor, *3rd International Conference on Computational Modeling and Simulation of Materials, Part A*, edited by F. Vincenzini, and A. Lami, Techna Group Srl., 481–488 2004.
[39] W. Zhong, G. Overney, and D. Tomanek, Phys. Rev. B **47**, 95 (1993).
[40] V. Heine, Phys. Rev. **153**, 673 (1967).
[41] O. K. Andersen, Solid State Commun. **13**, 133 (1973).
[42] C. Kittel, *Introduction to Solid State Physics*, 6th ed. (Wiley, New York, 1987); M. Acet, H. Zähres, E. F. Wassermann, and W. Pepperhoff, Phys. Rev. B **49**, 6012 (1994).
[43] S. Chantasiriwan and F. Milstein, Phys. Rev. B **58**, 5996 (1998).
[44] G. Y. Guo and H. H. Wang, Chin. J. Phys. (Taipei) **38**, 949 (2000).
[45] M. W. Finnis, K. L. Kear, and D. G. Pettifor, Phys. Rev. Lett. **52**, 291 (1984).
[46] P. J. Craievich, M. Weinert, J. M. Sanchez, and R. E. Watson, Phys. Rev. Lett. **72**, 3076 (1994).

[47] G. Simonelli, R. Pasianot, and E. J. Savino, Phys. Rev. B **50**, 727 (1994).
[48] H. E. Schaefer, K. Maier, M. Weller, D. Herlach, A. Seeger, and J. Dieht, Scr. Metall. **11**, 803 (1977).
[49] L. De Schepper, D. Segers, L. Dorikens-Vanpraet, M. Dorikens, G. Knuyt, L. M. Stals, and P. Moser, Phys. Rev. B **27**, 5257 (1983).
[50] P. Erhart, K. H. Robrock, and H. R. Schöber, in *Physics of Radiation Effects in Crystals*, edited by R. A. Johnson and A. N. Orlov (Elsevier, Amsterdam, 1986), p. 63.
[51] Chu-Chun Fu, F. Willaime, and P. Ordejon, Phys. Rev. Lett. **92**, 175503 (2004).
[52] D. Nguyen-Manh, D. G. Pettifor, and V. Vitek, Phys. Rev. Lett. **85**, 4136 (2000).